Structural insight into DNA-assembled oligochromophores: Crystallographic analysis of pyrene- and phenanthre....

Article *in* Nucleic Acids Research · July 2016

DOI: 10.1093/nar/gkw644

CITATIONS
0

READS
38

6 authors, including:

Walter Aeschimann
Universität Bern
16 PUBLICATIONS **15** CITATIONS
SEE PROFILE

Thi Thu Hang Chau
Universität Bern
2 PUBLICATIONS **0** CITATIONS
SEE PROFILE

Achim Stocker
Universität Bern
73 PUBLICATIONS **1,973** CITATIONS
SEE PROFILE

Nucleic Acids Research Advance Access published July 15, 2016

doi: 10.1093/nar/gkw644

Structural insight into DNA-assembled oligochromophores: crystallographic analysis of pyrene- and phenanthrene-modified DNA in complex with BpuJI endonuclease

Markus Probst, Walter Aeschimann, Thi T.H. Chau, Simon M. Langenegger, Achim Stocker* and Robert Häner*

Department of Chemistry and Biochemistry, University of Bern, 3012 Bern, Switzerland

Received June 16, 2016; Revised July 7, 2016; Accepted July 8, 2016

ABSTRACT

The use of the DNA duplex as a supramolecular scaffold is an established approach for the assembly of chromophore aggregates. In the absence of detailed structural insight, the characterization of thus assembled oligochromophores is, today, largely based on solution-phase spectroscopy. Here, we describe the crystal structures of three DNA-organized chromophore aggregates. DNA hybrids containing non-nucleosidic pyrene and phenanthrene building blocks were co-crystallized with the recently described binding domain of the restriction enzyme BpuJI. Crystal structures of these complexes were determined at 2.7, 1.9 and 1.6 Å resolutions. The structures reveal aromatic stacking interactions between pyrene and/or phenanthrene units within the framework of the B-DNA duplex. In hybrids containing a single modification in each DNA strand near the end of the duplex, the two polyaromatic hydrocarbons are engaged in a face-to-face stacking orientation. Due to crystal packing and steric effects, the terminal GC base pair is disrupted in all three crystal structures, which results in a non-perfect stacking arrangement of the aromatic chromophores in two of the structures. In a hybrid containing a total of three pyrenes, crystal lattice induced end-to-end stacking of individual DNA duplexes leads to the formation of an extended aromatic π-stack containing four co-axially arranged pyrenes. The aromatic planes of the stacked pyrenes are oriented in a parallel way. The study demonstrates the value of co-crystallization of chemically modified DNA with the recombinant binding domain of the restriction enzyme BpuJI for obtaining detailed structural insight into DNA-assembled oligochromophores.

INTRODUCTION

The DNA duplex represents a versatile framework for the assembly and study of supramolecular aggregates. The sequence-controlled self-assembly of DNA strands has resulted in an astonishing diversity of nano-architectures (1–11). The wide variety of modified building blocks available nowadays (12–27) allows the DNA-controlled assembly of multiple types of functional units, including aromatic chromophores (27–37). We recently described the construction of DNA-based light-harvesting antennas, in which non-nucleosidic phenanthrene and pyrene chromophores were organized in a sequence-defined manner (38–40). Solution-phase spectroscopy (41–43) and molecular dynamics simulations (44) strongly suggest that the polyaromatic chromophores are arranged via interstrand π-stacking. In-depth structural information on the nature of intra- and/or interstrand stacking interactions, however, is missing. Several x-ray crystallographic and solution nuclear magnetic resonance (NMR) structures have been reported on backbone-modified nucleic acids [see e.g. (45–47) and references cited therein; (48–51)] or on sugar-linked aromatic modifications [see (23) and references cited therein; (52–56)]. A lectin-bound fucosylated DNA duplex bearing two interacting sugar-linked phenanthrenes was published recently (57). On the other hand, structural data on the intrahelical organization of non-nucleosidic, polyaromatic hydrocarbons (PAHs) is limited to a single NMR-study by Nielsen *et al.* (58) highlighting the intra- and interhelical stacking interactions of two pyrene molecules attached via non-nucleosidic linkers. Further knowledge of the spatial arrangement of non-nucleosidic PAHs is crucial for a better comprehension of the properties of chromophore aggregates and a model based on experimental three-dimensional

*To whom correspondence should be addressed. Tel: +41 31 631 4382; Fax: +41 31 631 4272; Email: robert.haener@dcb.unibe.ch
Correspondence may also be addressed to Achim Stocker. Tel: +41 31 631 4315; Fax: +41 31 631 4887; Email: achim.stocker@dcb.unibe.ch

data will greatly improve our understanding of their molecular interactions within a DNA scaffold. To gain crystallographic insight into the intrahelical organization of non-nucleosidic oligochromophores we set out to co-crystallize chemically modified DNA with a suitable DNA-binding protein. Searching protein data bank (PDB) (www.rcsb.org) for mixed protein–DNA-type polymers led us to a recent high resolution structure involving the recognition domain of BpuJI obtained after thermolysin digestion (59,60). The stable N-terminal domain of this nuclease was used for co-crystallization of double helical DNA leading to a high resolution structure. Here, we report the successful co-crystallization of phenanthrene and/or pyrene modified DNA double helices as complexes with the DNA binding domain of BpuJI restriction endonuclease. Applying this approach to different PAH-modified duplexes resulted in three well-resolved structures described below.

MATERIALS AND METHODS

Cloning of the BpuJI binding domain

The N-terminal DNA binding domain (residues 1–285) of the BpuJI restriction endonuclease (59) was back-translated and optimized for codon usage in *Escherichia coli* with the help of the EMBOSS Backtranseq application (see Supplementary Data). After adding Nde1 (N-terminal) and Xho1 (C-terminal) restriction sites as well as a stop codon (TAA), the pre-designed sequence was synthesized by a commercial supplier (Bio Basic Canada Inc., Ontario, Canada). The synthetic DNA insert was isolated as linear fragment from the pUC57 cloning vector by restriction digestion (Nde1/Xho1) and ligated into the pET28a expression vector. The identity of the subcloned construct was confirmed by sequencing (Microsynth, Balgach, Switzerland).

Synthesis of the modified oligonucleotides

Synthesis of the pyrene and phenanthrene phosphoramidites and their incorporation into DNA oligonucleotides was accomplished as described in the literature (61,62). The purification and characterization of the strands was done by HPLC and analysis by electrospray ionization mass spectrometry, respectively (Supplementary Data). Three DNA duplexes were prepared with the single strands shown in Figure 1: 5′-G**Y**T ACC CGT GGA (**ON1**); 5′-TCC ACG GGT A**Y**C (**ON2**); 5′-G**Y**A CCC GTG GA (**ON3**); 5′-TCC ACG GGT **α**C (**ON4**); 5′-TCC ACG GGT **YY**C (**ON5**); where **Y** = 1,8-dibutynylpyrene and **α** = 3,6-dibutynylphenanthrene.

Expression and loading of the BpuJI DNA binding domain

The recombinant $\Delta_{1\text{-}285}$BpuJI protein (ΔBpuJI) was expressed in *E. coli* (transformed BL21 DE3) using ZYP-5052 rich medium for auto-induction. The cells were harvested by centrifugation at 10 000 *g* and suspended in lysis buffer (10 mM potassium phosphate buffer pH 7.4; 300 mM NaCl; 15 mM imidazole; 0.025% Triton X-100). The cells were disrupted by a French Press, centrifuged at 30 000 *g* and the supernatant was loaded onto a Ni-NTA column (affinity chromatography). The subsequent washing (lysis buffer,

ON1	5′- G**Y**T ACC CGT GGA -3′
ON2	3′- C**Y**A TGG GCA CCT -5′
ON3	5′- G**Y**A CCC GTG GA -3′
ON4	3′- C**α**T GGG CAC CT -5′
ON3	5′- G **Y** ACC CGT GGA -3′
ON5	3′- C**YY** TGG GCA CCT -5′

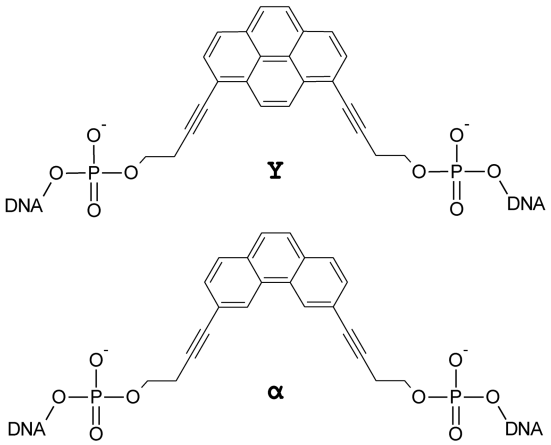

Figure 1. Sequences of modified oligonucleotides and chemical structures of the non-nucleosidic building blocks (**Y** = 1,8-dibutynylpyrene and **α** = 3,6-dibutynylphenanthrene).

except for imidazole → 40 mM) and elution (lysis buffer, except for imidazole → 200 mM) steps were performed at 4°C. The eluate usually contained about 0.5–0.6 mg protein per ml. Based on the protein concentration of the eluate a 1.1 molar excess of a corresponding DNA duplex was added. DNA duplexes consisted of either **ON1*ON2**, **ON3*ON4** or **ON3*ON5** modified single strands respectively. The modified single strands were prepared and annealed in an aqueous solution containing 100 mM NaCl and 10 mM sodium phosphate buffer (pH 7.4) prior to protein–DNA complex formation. Finally, thrombin was added to the samples and cleavage of the His-tag was allowed to occur overnight at 4°C.

Purification and crystallization screens

The samples were concentrated to a smaller volume and subjected to gel filtration [Superdex 200 10/300 GL; buffer A: 10 mM Tris–HCl pH 7.5; 0.1 mM ethylenediaminetetraacetic acid; 1 mM DL-dithiothreitol (DTT); 0.02% NaN_3]. All samples showed two major peaks in the chromatogram. Only the fractions from the first peak were pooled and concentrated to a final concentration of 5 mg complex per ml (for ΔBpuJI:**ON1*ON2**), 6 mg complex per ml (for ΔBpuJI:**ON3*ON4**) and 10 mg complex per ml (for ΔBpuJI:**ON3*ON5**). Crystallization was carried out by the sitting-drop method using PEG/Ion and PEG/Ion 2 screens from Hampton Research. For ΔBpuJI:**ON1*ON2**, the best crystals were grown in drops consisting of 1 μl

complex in buffer A and 1 μl of the reservoir solution (0.2 M magnesium acetate tetrahydrate; 20% w/v polyethylene glycol 3350). In case of ΔBpuJI:**ON3*ON4**, the best crystals were obtained from 2 μl of complex in buffer A and 1 μl of reservoir solution (0.2 M ammonium citrate tribasic 7.0; 20% w/v polyethylene glycol 3350). For ΔBpuJI:**ON3*ON5**, the best crystals formed from a 2:1 drop of the solution containing the complex and the reservoir solution (8% v/v Tacsimate 6.0; 20% w/v polyethylene glycol 3350). Cryo-protection was achieved by adding 20% w/v glycerol to the corresponding reservoir solution.

Data collection and structure determination

Diffraction datasets were collected at the X06DA beamline at the Swiss Light Source (SLS, Paul Scherrer Institut, Villigen, Switzerland). Data were processed using XDS (63). The PHENIX software suite (64) and Coot (65) were used for model building and refinement. First, Phaser-MR (66) and AutoBuild (67) were used in order to create an initial model of the structure, based on the existing PDB code: 2VLA. The natural nucleotides that were not present in our oligonucleotide sequences were removed from the initial model and replaced stepwise with the non-nucleosidic pyrene and phenanthrene components. Data files containing the geometry restraints of these molecules were generated using the PRODRG Server (68). An additional file describing the bonds between artificial and natural building blocks had to be written and included in the refinement process.

RESULTS AND DISCUSSION

X-ray structure determination of protein–DNA complexes

The major goal of the present study was to elucidate intra- and interstrand interaction modes of non-nucleosidic polyaromatic building blocks within a DNA double helical framework. The DNA-binding domain (ΔBpuJI) of the type IIS restriction endonuclease BpuJI was chosen as a prototypical B-DNA binder for co-crystallization with pyrene- and phenanthrene-modified DNA duplexes. X-ray structural data of ΔBpuJI complexed with a 12 base pair DNA duplex recently showed specific recognition of a 5′-CCCGT target sequence, located at the central position of the duplex, by the endonuclease and lack of interference with the terminal nucleosides (59). The BpuJI–DNA interactions exclusively occur in the major groove of the DNA and preserve the canonical B-form of the duplex. We hypothesized that unnatural building blocks located distal to the 5′-CCCGT target sequence should be best tolerated within the prototypical BpuJI:DNA binding mode. Accordingly, three different sets of mutually complementary oligonucleotides, containing a central BpuJI sequence and pyrene (**Y**) and phenanthrene (**α**) modifications next to the terminal GC base pair (Figure 1), were designed and prepared according to previously established methods.

The pre-annealed PAH-modified duplexes were mixed with freshly prepared ΔBpuJI at a 1.1 molar excess of DNA over protein. The resulting ΔBpuJI:DNA adducts were isolated as protein–DNA complexes by size exclusion chromatography and, after adjusting for the concentration of the complexes, directly used in sitting drop crystallization experiments. For the three binary protein–DNA complexes described herein, highly diffracting crystals were obtained. Subsequently, crystal structures of these complexes were determined at 2.7, 1.6 and 1.9 Å resolution (Table 1). All structures were solved by molecular replacement based on the existing PDB code: 2VLA of BpuJI. Relevant data collection and refinement parameters are listed in Table 1.

The complex with the 12-mer duplex **ON1*ON2** contains two non-nucleosidic pyrene building blocks placed oppositely in position 2 (next to the terminal GC base pair, see Figure 1), while the complex with the 11-mer duplex **ON3*ON4** has one pyrene and one phenanthrene in the same position. The third complex contains a DNA hybrid formed of an 11-mer and a 12-mer (**ON3*ON5**) and comprises three pyrenes arranged adjacently to the terminal GC base pair as illustrated in Figure 1.

Crystal structure of duplex ON1*ON2: pyrene–pyrene interactions

Crystals of complex ΔBpuJI:**ON1*ON2** showed orthorhombic symmetry, and the data were collected at a resolution of 2.67 Å. The asymmetric unit (ASU) contains two ΔBpuJI DNA binding domains. Each is bound to an individual **ON1*ON2** duplex that exhibits a regular B-DNA conformation (Figure 2).

Overall, both ΔBpuJI:**ON1*ON2** complexes are virtually indistinguishable from their native BpuJI:B-DNA counterpart (R.m.s. deviation = 0.444 Å, Supplementary Data), with the exception of the newly introduced non-nucleosidic 1,8-dialkynypyrene building blocks and the terminal GC base pair. The latter is disrupted due to the increased steric demand of the pyrene-modified duplex in comparison to the parent native duplex (59). The increased steric demand is a result of an interstrand stacking arrangement of the two pyrenes, leading to an extension of the duplex in this region (see below for further explanation). The intact B-DNA conformation indicates that replacing nucleosidic building blocks distal to the 5′-CCCGT target sequence of BpuJI is well tolerated and maintains a B-form of the modified duplex within the complex.

In the region of the non-nucleosidic building blocks, the electron density covers the majority of the aromatic ring structures of both covalently attached pyrenes and the ring orientation is well-defined. The first pyrene moiety stacks right on top of the last Watson–Crick base pair (see Figure 3). Due to the relatively strong density of the phosphate groups, the remaining pyrene and the 5′ guanine of **ON1** could be placed by following the backbone of the strands. In contrast to the phosphate groups, almost no density is present along the butynyl linkers and the 3′-cytidine of **ON2**, suggesting that these regions of the duplex are significantly disordered.

The two pyrene units of the ΔBpuJI:**ON1*ON2** complex are in close contact with each other. Their arrangement can be described as a displaced, face-to-face stacking interaction. The proximity of the two pyrenes is in agreement with the observed excimer fluorescence in solutions of DNA hybrids containing 1,8-linked, non-nucleosidic pyrenes in opposite positions (41,61,69). However, the orientation of the

Table 1. Data collection and refinement statistics for protein–DNA complexes

	ΔBpuJI:**ON1*ON2**	ΔBpuJI:**ON3*ON4**	ΔBpuJI:**ON3*ON5**
Data collection			
Temperature (K)	100	100	100
X-ray wavelength (Å)	1.000010	1.000040	1.000040
Space group	P 21 21 21 (19)	C 1 2 1 (5)	P 21 21 2 (18)
Cell dimensions:			
a, b, c (Å)	77.87, 85.50, 115.90	165.72, 59.28, 44.05	44.03, 59.67, 164.40
α, β, γ (°)	90.00, 90.00, 90.00	90.00, 94.20, 90.00	90.00, 90.00, 90.00
Resolution (Å)*	2.67–47.97 (2.83–2.67)	1.55–43.93 (1.64–1.55)	1.88–48.29 (1.99–1.88)
Completeness (%)*	94.5 (89.5)	98.0 (95.1)	97.3 (90.8)
I/Sigma I*	12.89 (1.70)	16.70 (3.03)	14.14 (1.93)
R-meas (%)*	6.6 (57.8)	5.5 (44.9)	5.6 (67.2)
CC (1/2)*	99.8 (68.0)	99.9 (84.3)	99.9 (77.7)
Refinement			
Resolution (Å)	2.67–46.49	1.55–43.93	1.88–48.29
Reflections (non-anomalous)	22 202	61 042	35 452
R_{work}/R_{free}	0.2007 / 0.2436	0.1706/0.1955	0.1691/0.1995
Number of non-H atoms:			
Protein/DNA	5367	2800	2771
Water	50	479	171
Average B ($Å^2$)	64.8	24.7	44.0
R.m.s. deviations:			
Bonds (Å)	0.003	0.011	0.009
Angles (°)	0.6	1.2	1.0

*Statistics for the highest-resolution shell are shown in parentheses.

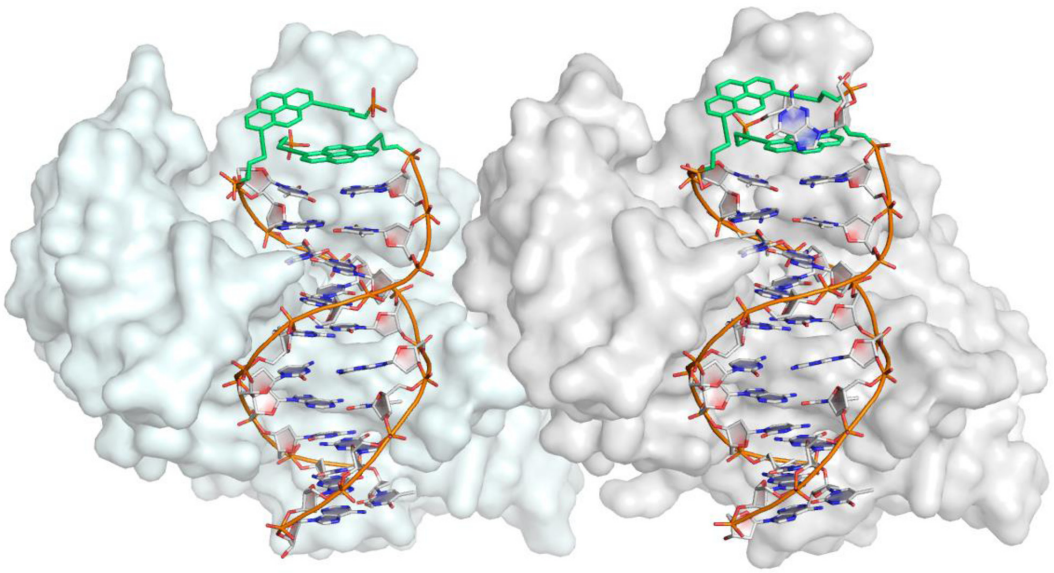

Figure 2. Structure of the two ΔBpuJI:**ON1*ON2** complexes in the asymmetric unit (ASU). DNA binding domains are represented as gray protein surfaces. The phosphate backbones of the DNA (orange tubes) are linked to the pyrene units (green).

two aromatic planes is not parallel, as might be expected, but wedged (25–30°). Interestingly, each modified duplex of the ΔBpuJI:**ON1*ON2** complex is connected to its neighbor in a head-to-tail fashion forming a linear DNA array in the crystal lattice. In this DNA array, each terminal pyrene is involved in direct crystal contacts with the next duplex by stacking to the adjacent terminal TA base pair (Figure 4). The parallel alignment of the pyrene and this TA base pair suggests that this interaction is more important, at least in the crystal, than the stacking between the two pyrenes and, thus, provides a rationale for the non-perfect, wedged pyrene–pyrene stacking interaction. Furthermore, the end-to-end contacts between the duplexes of two adjoining complexes show a similarity with the published complex (59), in which tight coaxial stacking of individual duplexes was also found. These end-to-end stacking interactions appear to be important for the formation of the crystal lattice.

Crystal structure of duplex ON3*ON4: pyrene–phenanthrene interactions

In contrast to the orthorhombic crystals of two ΔBpuJI-bound **ON1*ON2** 12-mer duplexes, crystals of the

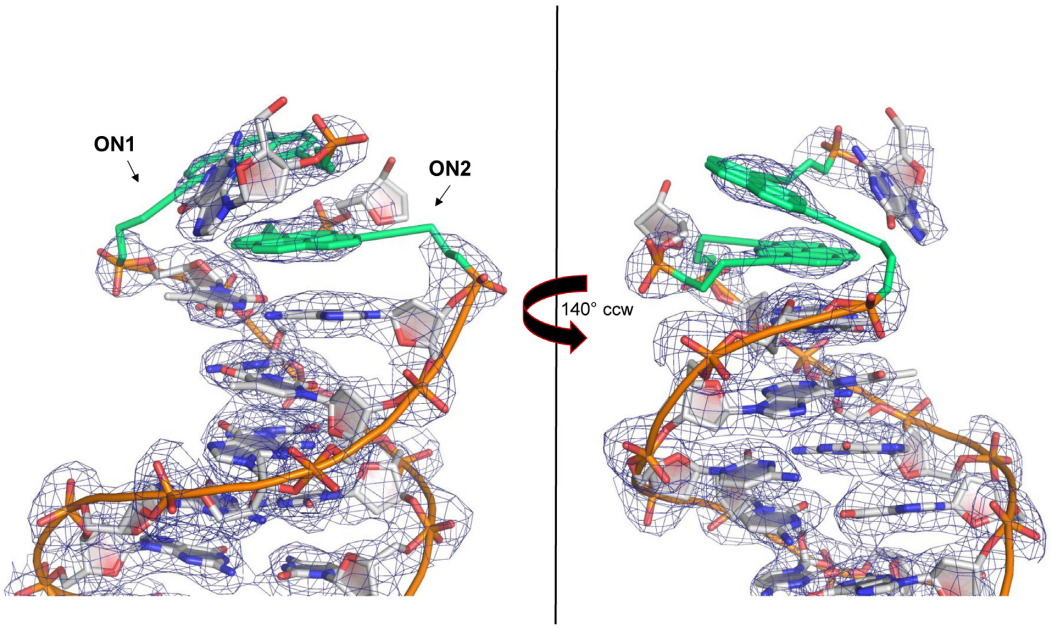

Figure 3. Close-up view of the terminal region of the **ON1*ON2** duplex. The **ON2** pyrene stacks on top of the last Watson–Crick base pair in the DNA duplex. The 3′-terminal cytidine of **ON2** could not be positioned (left image). Right image: left view turned counterclockwise by 140° toward the viewer for better visualization of the pyrene building blocks and the guanine at the 5′-end of **ON1**. Views are shown with the $2F_o–F_c$ map contoured at 1 σ level and omitting the protein surface.

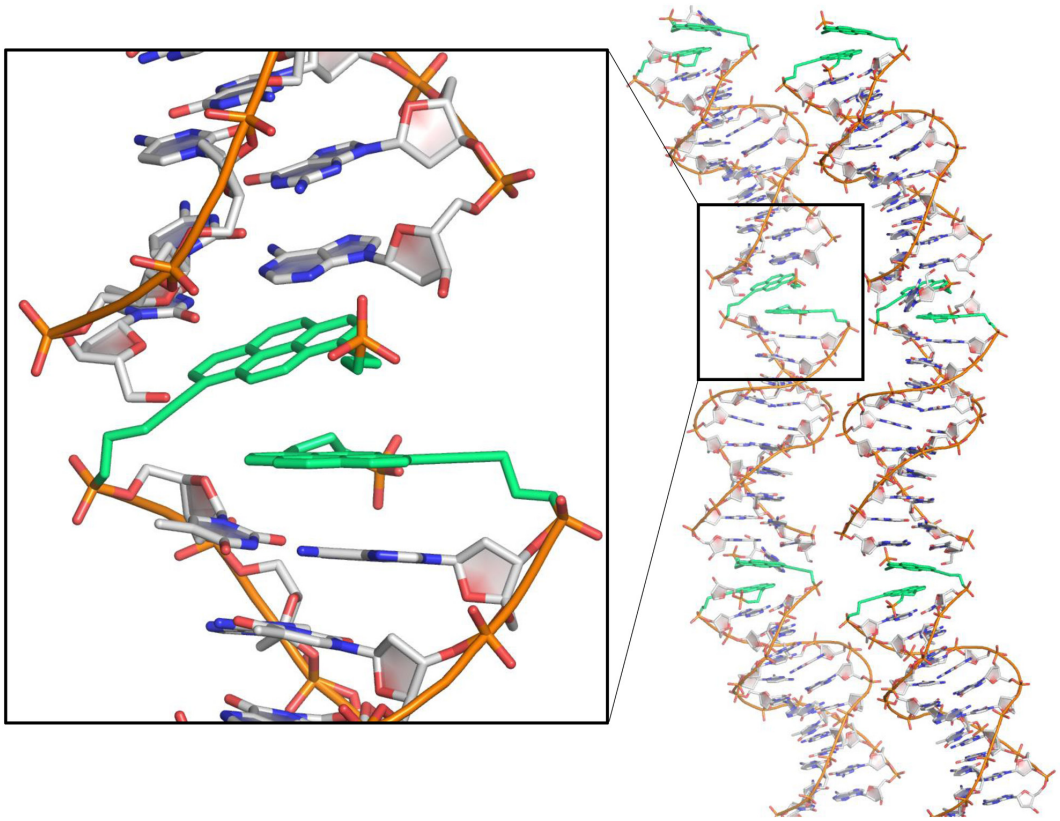

Figure 4. Head-to-tail arrangement of the duplexes throughout the crystal lattice of the ΔBpuJI:**ON1*ON2** complex. The protein moieties are omitted for better visibility of the DNA array. The inset depicts the stacking interactions between pyrenes and nucleobases.

ΔBpuJI:**ON3*ON4** complex were found to have monoclinic symmetry with a single moiety bound to one 11-mer **ON3*ON4** duplex in the ASU. The high resolution of 1.55 Å allowed for an easy assignment of the nucleotides and the aromatic phenanthrene ring within the electron density map (Figures 5 and 6).

The pyrene and phenanthrene building blocks within the BpuJI binding site are separated by only one base pair from the 5′-CCCGT binding sequence. Nevertheless, the B-DNA conformation is preserved in the BpuJI DNA binding domain of the **ON3*ON4** duplex. The electron density in the region of the covalently attached phenanthrene building block nicely covers the aromatic ring moiety, including its butynyl linkers and the connecting phosphate group (Figure 6).

The phenanthrene ring stacks on top of the last Watson–Crick base pair. The electron density of the pyrene moiety of **ON3** is well enough defined for establishing its ring orientation and reveals a stacking interaction with the phenanthrene. The terminal 3′-C of **ON4** points away from the helical axis, whereas the terminal 5′-G of **ON3** may be arranged in a stacking interaction with the pyrene. Both nucleotides, however, reveal a comparably weak electron density, indicating that the terminal nucleotides of the duplex are largely disordered. The disruption of the terminal GC base pair is explained by steric clashes resulting from the elongation of the DNA duplex by the incorporated aromatic building blocks. In contrast to the head-to-tail linear arrangement observed for ΔBpuJI:**ON1*ON2**, the complex ΔBpuJI:**ON3*ON4** reveals a head-to-head type interaction between adjacent helices in the crystal lattice (Figure 7). The interaction of two neighboring helices is not mediated by PAH stacking interactions, as might be expected, because the two pyrenes are spatially well separated.

Crystal structure of duplex ON3*ON5: extended coaxial pyrene stacks

The ΔBpuJI:**ON3*ON5** structure contains a total of three pyrene building blocks: strand **ON3** has one pyrene in position 2 and strand **ON5** has two pyrenes in positions 2 and 3 (Figure 8). Two strong electron densities on top of the last natural base pair reveal that the two pyrenes of strand **ON5** are arranged in an intrastrand stacking interaction. The single pyrene moiety of strand **ON3** and the adjacent terminal 5′-G are shifted aside from the stack, which can be explained by steric factors imposed by the crystal lattice. The comparatively weak density suggests a relatively large disorder in this region. Also the terminal 3′-C of **ON5** is disordered and could not be identified within the present density map. Crystals of ΔBpuJI:**ON3*ON5** disclose a head-to-head type coaxial stacking interaction between adjacent DNA duplexes. The contact between the two DNA duplexes occurs via pyrene–pyrene contacts, thus leading to an extended pyrene stack composed of four units (Figure 9). Aromatic planes of the pyrenes are aligned in a parallel, face-to-face stacking mode. The stacking distances between adjacent pyrenes is 3.5 Å. The terminal GC base pair is also disrupted in this structure. This leads to the formation of dangling ends: a pyrene and a G on the 5′-end and a 3′-C. The 5′-terminal guanine is engaged in a *trans Hoogsteen/sugar edge* type base pair (70) with a nearby adenine (see Supplementary Data).

The data obtained in this study demonstrate that non-nucleosidic PAHs, such as phenanthrene and pyrene engage in intra- and interstrand stacking interactions inside a DNA double helical framework. The findings support the spectroscopic data previously obtained in solution with pyrene and phenanthrene modified DNAs. This includes, in particular, excimer formation among pyrenes placed in opposite positions in a DNA double helix or arranged in adjacent positions in the same strand. In addition, the importance of stacking interactions between the PAH and the natural base pairs is further underlined by all three structures. End-to-end stacking of alkynyl substituted PAHs is observed in crystal lattices and seems to play a major role in cases where interhelical stacking is possible. Such oligo- or polymerization has been observed previously for phosphodiester-linked oligomers, not only for pyrene (71) or phenanthrene (62), but also for DNA containing other chromophores, such as perylenediimide (72) or porphyrins (73). In all the three structures described here, the non-natural building blocks are involved in head-to-head or head-to-tail contacts between the protein–DNA complexes in the crystal lattice. The non-modified parts of the DNA duplexes remain in their canonical B-DNA conformation in all the three structures and the binding region, as well as the rest of the protein, are identical to the reference structure (59). Furthermore, the typical changes observed in the vibronic patterns in UV/vis absorption bands (74) of stacked pyrenes are also maintained in the three duplexes when they are complexed to ΔBpuJI (see Supplementary Data). Thus, ΔBpuJI appears as an ideal system for co-crystallization of not only canonical but also chemically modified DNA duplexes. Crystallization attempts with ΔBpuJI bound to DNA duplexes bearing modifications in the DNA binding region (i.e. in the central region of the duplex) were, so far, unsuccessful.

CONCLUSIONS

The incorporation of non-nucleosidic building blocks into DNA results in constructs with distinct structural and electronic properties. In the present study, we describe the structural details of non-nucleosidic dialkynylpyrenes and dialkynylphenanthrenes in a DNA double helical framework. Three modified duplexes were investigated by x-ray analysis after co-crystallization with the recombinant binding domain of the restriction enzyme BpuJI (59). In the binary complex, the DNA serves as a scaffold for the molecular organization of the chromophores and provides a recognition site for the DNA binding part of the protein. The overall B-DNA conformation of the parent duplex is maintained in the presence of the terminally attached modified building blocks. The structures elucidate the nature of the stacking interactions between the pyrene and/or phenanthrene units. In duplexes containing one modification in each DNA strand near the end of the duplex, the two chromophores are engaged in a face-to-face stacking orientation, albeit not in a perfectly parallel arrangement. Crystal packing effects and steric clashes resulting from the elongation of the DNA duplex by the incorporated aromatic

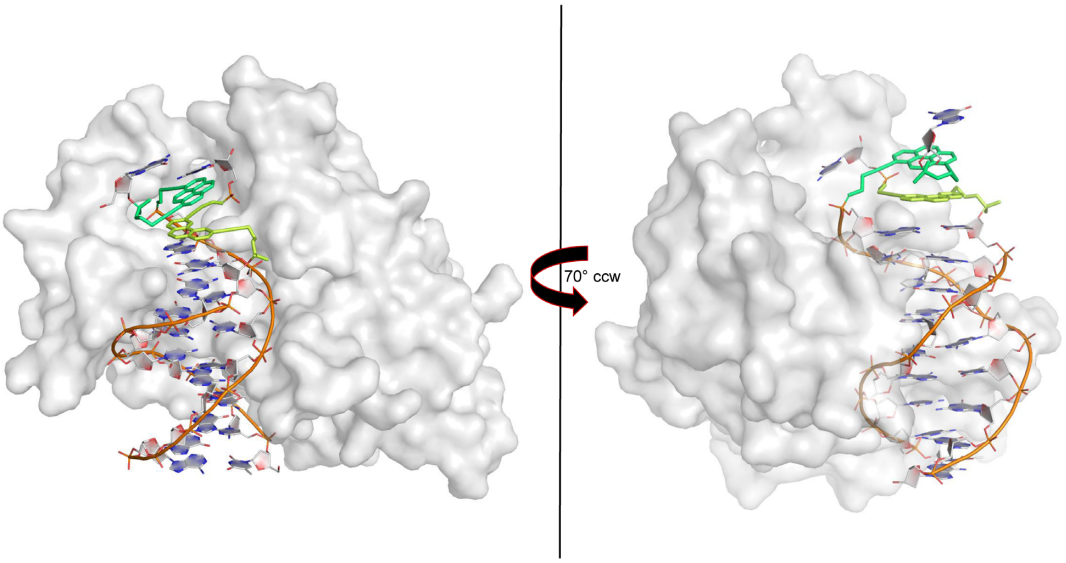

Figure 5. Structure of the ΔBpuJI:**ON3*ON4** complex. The protein is represented as a gray surface. The phosphate backbone of the DNA (orange tubes) is linked to the phenanthrene (lime) and pyrene (green) modifications.

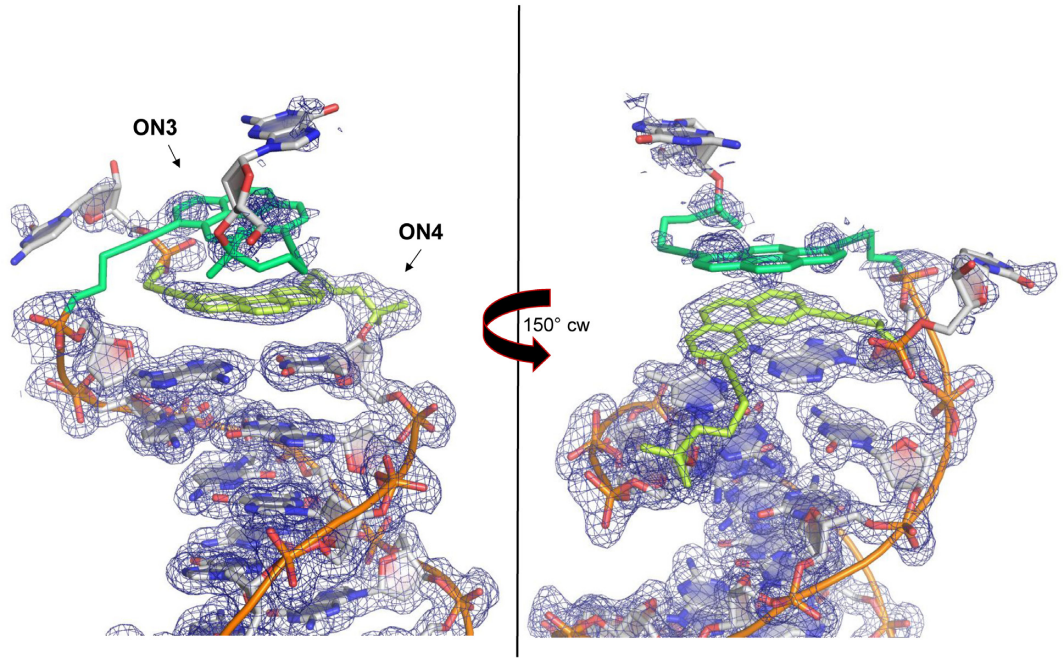

Figure 6. Close-up view of the terminal region of complex ΔBpuJI:**ON3*ON4**. The phenanthrene is stacked onto the last Watson–Crick base pair, the cytidine at the 3′-end of **ON4** points away from the helical axis. Views are shown with the $2F_o–F_c$ map contoured at 1 σ level (except for pyrenes and terminal nucleotides, for which $\sigma = 0.8$) and omitting the protein surface.

building blocks are at least partly responsible for the non-perfect stacking interactions in duplexes **ON1*ON2** and **ON3*ON4**. The presence of steric effects is demonstrated by the fact that the terminal GC base pairs are disrupted in all the three crystal structures. In duplex **ON3*ON5**, crystal-lattice-induced end-to-end stacking of individual DNA duplexes leads to the formation of an extended aromatic π-stack of four co-axially arranged pyrenes. The aromatic planes of the stacked pyrenes are oriented in a parallel manner. The single pyrene present in **ON3** is separated from the pyrene stack, which can again be explained by steric factors imposed by the crystal lattice. This study demonstrates the value of co-crystallization of chemically modified DNA with the recombinant binding domain of the restriction enzyme BpuJI for obtaining otherwise inaccessible structural information about DNA-assembled oligochromophores.

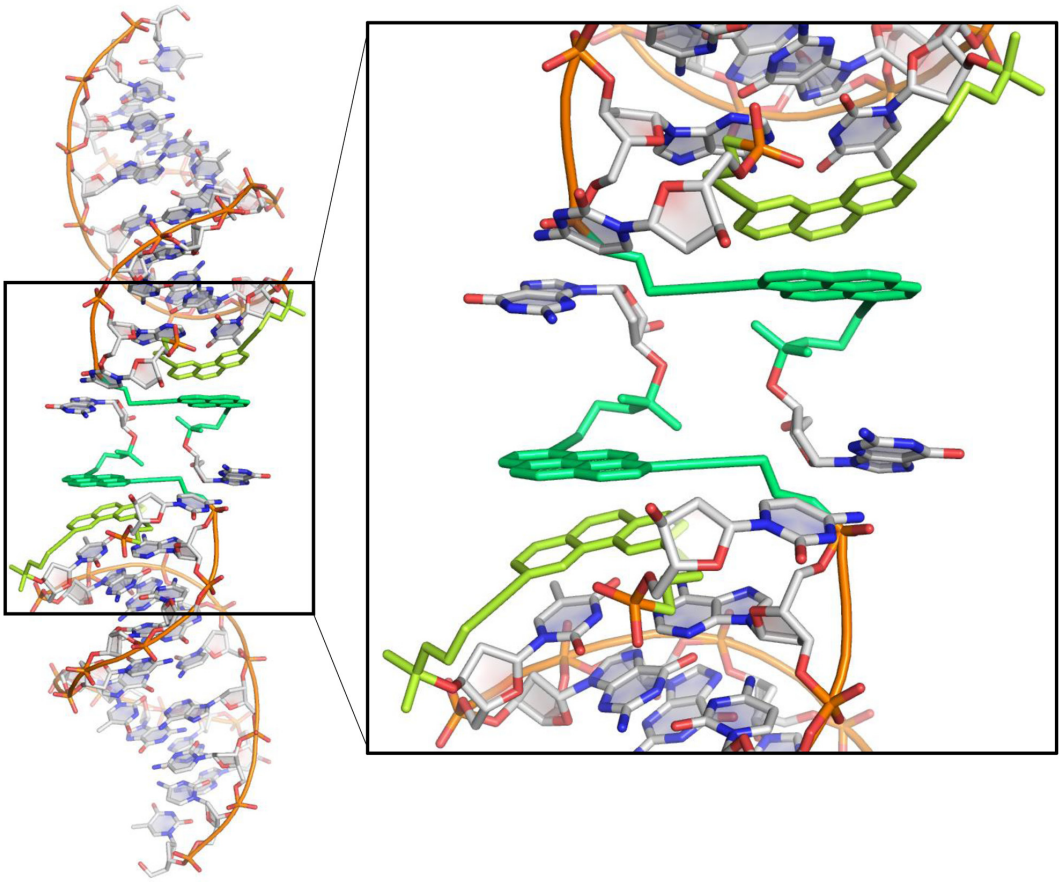

Figure 7. Repetition of the duplex throughout the crystal lattice of complex ΔBpuJI:**ON3*ON4** highlighting the head-to-head type interaction between adjacent helices.

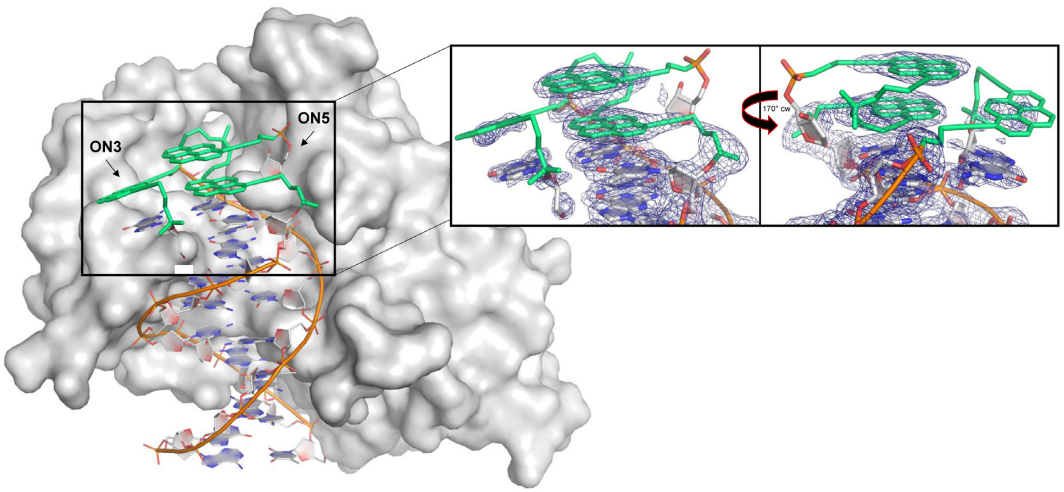

Figure 8. Structure of complex ΔBpuJI:**ON3*ON5** in the ASU (protein surface gray, DNA phosphate backbone orange and pyrenes green).

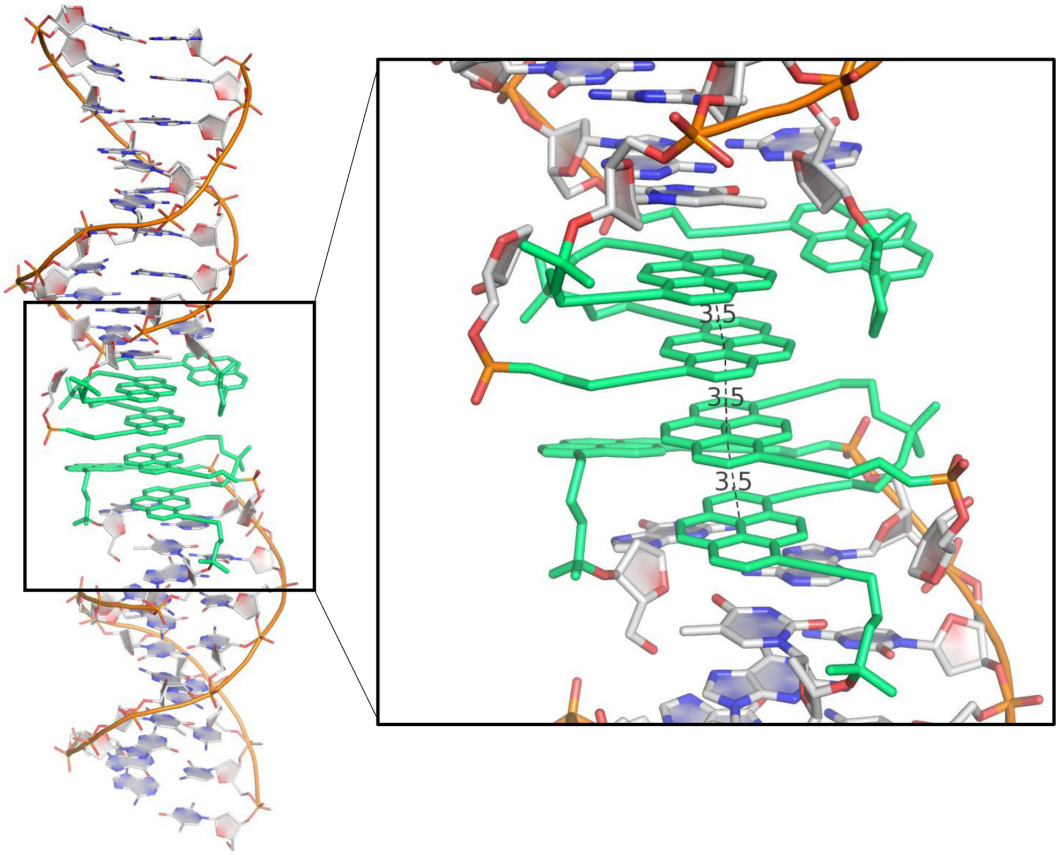

Figure 9. Head-to-head arrangement of DNA duplexes in the ΔBpuJI:**ON3*ON5** crystal lattice. The most notable feature of this structure is the formation of an extended stack of four pyrene units (two from each protein–DNA complex). The single pyrene of **ON3** (arrow) forms a dangling end together with the adjacent 5′-terminal guanosine and is thus separated from the pyrene stack.

ACCESSION NUMBERS

Crystallographic models of the three complexes have been deposited in the PDB (http://www.rcsb.org, PDB codes: 5HLT, 5HNF, 5HNH).

SUPPLEMENTARY DATA

Supplementary Data are available at NAR Online.

ACKNOWLEDGEMENT

We gratefully acknowledge beam time and support at the Swiss Light Source (PSI, Villigen, Switzerland).

FUNDING

Swiss National Foundation [200020_149148]. Funding for open access charge: Department of Chemistry and Biochemistry, University of Bern.
Conflict of interest statement. None declared.

REFERENCES

1. Jones,M.R., Seeman,N.C. and Mirkin,C.A. (2015) Programmable materials and the nature of the DNA bond. *Science*, **347**, 1260901.
2. Torring,T., Voigt,N.V., Nangreave,J., Yan,H. and Gothelf,K.V. (2011) DNA origami: a quantum leap for self-assembly of complex structures. *Chem. Soc. Rev.*, **40**, 5636–5646.
3. Sacca,B. and Niemeyer,C.M. (2012) DNA origami: the art of folding DNA. *Angew. Chem. Int. Ed.*, **51**, 58–66.
4. McLaughlin,C.K., Hamblin,G.D. and Sleiman,H.F. (2011) Supramolecular DNA assembly. *Chem. Soc. Rev.*, **40**, 5647–5656.
5. Endo,M., Yang,Y. and Sugiyama,H. (2013) DNA origami technology for biomaterials applications. *Biomater. Sci.*, **1**, 347–360.
6. Tintore,M., Eritja,R. and Fabrega,C. (2014) DNA nanoarchitectures: steps towards biological applications. *Chembiochem*, **15**, 1374–1390.
7. Yang,D., Hartman,M.R., Derrien,T.L., Hamada,S., An,D., Yancey,K.G., Cheng,R., Ma,M. and Luo,D. (2014) DNA materials: bridging nanotechnology and biotechnology. *Acc. Chem. Res.*, **47**, 1902–1911.
8. Wang,Z.G., Song,C. and Ding,B. (2013) Functional DNA nanostructures for photonic and biomedical applications. *Small*, **9**, 2210–2222.
9. Jester,S.S. and Famulok,M. (2014) Mechanically interlocked DNA nanostructures for functional devices. *Acc. Chem. Res.*, **47**, 1700–1709.
10. Albinsson,B., Hannestad,J.K. and Boerjesson,K. (2012) Functionalized DNA nanostructures for light harvesting and charge separation. *Coord. Chem. Rev.*, **256**, 2399–2413.
11. Rothemund,P.W.K. (2006) Folding DNA to create nanoscale shapes and patterns. *Nature*, **440**, 297–302.
12. Uhlmann,E. and Peyman,A. (1990) Antisense oligonucleotides - a new therapeutic principle. *Chem. Rev.*, **90**, 543–584.
13. Nielsen,P.E. and Haaima,G. (1997) Peptide nucleic acid (PNA). A DNA mimic with a pseudopeptide backbone. *Chem. Soc. Rev.*, **26**, 73–78.

14. De Mesmaeker,A., Häner,R., Martin,P. and Moser,H.E. (1995) Antisense oligonucleotides. *Acc. Chem. Res.*, **28**, 366–374.
15. Freier,S.M. and Altmann,K.H. (1997) The ups and downs of nucleic acid duplex stability: structure-stability studies on chemically-modified DNA:RNA duplexes. *Nucleic Acids Res.*, **25**, 4429–4443.
16. Kool,E.T. (2002) Replacing the nucleohases in DNA with designer molecules. *Acc. Chem. Res.*, **35**, 936–943.
17. Eschenmoser,A. (2005) Searching for nucleic acid alternatives. *Chimia*, **59**, 836–850.
18. Burley,G.A., Buurma,N.J., Wellner,C., Stubinitzky,C., Wagenknecht,H.A., Sinha,I., Müller,J., Takezawa,Y., Duprey,J.L. and Shionoya,M. (2014) (Non-) Covalently modified DNA with novel functions. In: Stulz,E and Clever,GH (eds). *DNA in Supramolecular Chemistry and Nanotechnology*. John Wiley & Sons, Chichester, pp. 1–77.
19. Astakhova,I.K. and Wengel,J. (2014) Scaffolding along nucleic acid duplexes using 2′-amino-locked nucleic acids. *Acc. Chem. Res.*, **47**, 1768–1777.
20. Herdewijn,P. (1999) Conformationally restricted carbohydrate-modified nucleic acids and antisense technology. *Biochim. Biophys. Acta Gene Struct. Expr.*, **1489**, 167–179.
21. Benner,S.A. (2004) Understanding nucleic acids using synthetic chemistry. *Acc. Chem. Res.*, **37**, 784–797.
22. Meggers,E. and Zhang,L. (2010) Synthesis and properties of the simplified nucleic acid glycol nucleic acid. *Acc. Chem. Res.*, **43**, 1092–1102.
23. Malyshev,D.A. and Romesberg,F.E. (2015) The expanded genetic alphabet. *Angew. Chem. Int. Ed.*, **54**, 11930–11944.
24. Takezawa,Y. and Shionoya,M. (2012) Metal-mediated DNA base pairing: alternatives to hydrogen-bonded Watson-Crick base pairs. *Acc. Chem. Res.*, **45**, 2066–2076.
25. Sinkeldam,R.W., Greco,N.J. and Tor,Y. (2010) Fluorescent analogs of biomolecular building blocks: design, properties, and applications. *Chem. Rev.*, **110**, 2579–2619.
26. Hottin,A. and Marx,A. (2016) Structural insights into the processing of nucleobase-modified nucleotides by DNA polymerases. *Acc. Chem. Res.*, **49**, 418–427.
27. Wojciechowski,F. and Leumann,C.J. (2011) Alternative DNA base-pairs: from efforts to expand the genetic code to potential material applications. *Chem. Soc. Rev.*, **40**, 5669–5679.
28. Teo,Y.N. and Kool,E.T. (2012) DNA-multichromophore systems. *Chem. Rev.*, **112**, 4221–4245.
29. Malinovskii,V.L., Wenger,D. and Häner,R. (2010) Nucleic acid-guided assembly of aromatic chromophores. *Chem. Soc. Rev.*, **39**, 410–422.
30. Kamiya,Y. and Asanuma,H. (2014) Light-driven DNA nanomachine with a photoresponsive molecular engine. *Acc. Chem. Res.*, **47**, 1663–1672.
31. Filichev,V.V. and Pedersen,E.B. (2009) DNA-conjugated organic chromophores in DNA stacking interactions. In: Begley,TP (ed). *Wiley Encycl.Chem.Biol.*, Wiley, Hoboken, Vol. **1**, pp. 493–524.
32. Bandy,T.J., Brewer,A., Burns,J.R., Marth,G., Nguyen,T., Stulz,E. and Soc,C. (2011) DNA as supramolecular scaffold for functional molecules: progress in DNA nanotechnology. *Chem. Soc. Rev.*, **40**, 138–148.
33. Ostergaard,M.E. and Hrdlicka,P.J. (2011) Pyrene-functionalized oligonucleotides and locked nucleic acids (LNAs): tools for fundamental research, diagnostics, and nanotechnology. *Chem. Soc. Rev.*, **40**, 5771–5788.
34. Varghese,R. and Wagenknecht,H.A. (2009) DNA as a supramolecular framework for the helical arrangements of chromophores: towards photoactive DNA-based nanomaterials. *Chem. Commun.*, 2615–2624.
35. Balaz,M., Bitsch-Jensen,K., Mammana,A., Ellestad,G.A., Nakanishi,K. and Berova,N. (2007) Porphyrins as spectroscopic sensors for conformational studies of DNA. *Pure Appl. Chem.*, **79**, 801–809.
36. Dohno,C. and Nakatani,K. (2011) Control of DNA hybridization by photoswitchable molecular glue. *Chem. Soc. Rev.*, **40**, 5718–5729.
37. Hovelmann,F. and Seitz,O. (2016) DNA stains as surrogate nucleobases in fluorogenic hybridization probes. *Acc. Chem. Res.*, **49**, 714–723.
38. Garo,F. and Häner,R. (2012) A DNA-based light-harvesting antenna. *Angew. Chem. Int. Ed.*, **51**, 916–919.
39. Probst,M., Langenegger,S.M. and Häner,R. (2014) A modular LHC built on the DNA three-way junction. *Chem. Commun.*, **50**, 159–161.
40. Adeyemi,O.O., Malinovskii,V.L., Biner,S.M., Calzaferri,G. and Häner,R. (2012) Photon harvesting by excimer-forming multichromophores. *Chem. Commun.*, **48**, 9589–9591.
41. Langenegger,S.M. and Häner,R. (2004) Excimer formation by interstrand stacked pyrenes. *Chem. Commun.*, 2792–2793.
42. Samain,F., Malinovskii,V.L., Langenegger,S.M. and Häner,R. (2008) Spectroscopic properties of pyrene-containing DNA mimics. *Bioorg. Med. Chem.*, **16**, 27–33.
43. Galievsky,V.A., Malinovskii,V.L., Stasheuski,A.S., Samain,F., Zachariasse,K.A., Häner,R. and Chirvony,V.S. (2009) Photophysical characterization of oligopyrene modules for DNA-based nanosystems. *Photochem. Photobiol. Sci.*, **8**, 1448–1454.
44. Simona,F., Nussbaumer,A.L., Häner,R. and Cascella,M. (2013) Supramolecular organization of heptapyrenotide oligomers-an in depth investigation by molecular dynamics simulations. *J. Phys. Chem. B*, **117**, 2576–2585.
45. Egli,M. and Pallan,P.S. (2010) The many twists and turns of DNA: template, telomere, tool, and target. *Curr. Opin. Struct. Biol.*, **20**, 262–275.
46. Anosova,I., Kowai,E.A., Dunn,M.R., Chaput,J.C., Van Horn,W.D. and Egli,M. (2016) The structural diversity of artificial genetic polymers. *Nucleic Acids Res.*, **44**, 1007–1021.
47. Egli,M. and Pallan,P.S. (2010) Crystallographic studies of chemically modified nucleic acids: a backward glance. *Chem. Biodiv.*, **7**, 60–89.
48. Yeh,J.I., Pohl,E., Truan,D., He,W., Sheldrick,G.M., Du,S. and Achim,C. (2010) The crystal structure of non-modified and bipyridine-modified PNA duplexes. *Chem. Eur. J.*, **16**, 11867–11875.
49. Schlegel,M.K., Essen,L.O. and Meggers,E. (2008) Duplex structure of a minimal nucleic acid. *J. Am. Chem. Soc.*, **130**, 8158–8159.
50. Lewis,F.D., Liu,X., Wu,Y., Miller,S.E., Wasielewski,M.R., Letsinger,R.L., Sanishvili,R., Joachimiak,A., Tereshko,V. and Egli,M. (1999) Structure and photoinduced electron transfer in exceptionally stable synthetic DNA hairpins with stilbenediether linkers. *J. Am. Chem. Soc.*, **121**, 9905–9906.
51. Patra,A. and Richert,C. (2009) High fidelity base pairing at the 3′-terminus. *J. Am. Chem. Soc.*, **131**, 12671–12681.
52. Guckian,K.M., Krugh,T.R. and Kool,E.T. (1998) Solution structure of a DNA duplex containing a replicable difluorotoluene-adenine pair. *Nat. Struct. Biol.*, **5**, 954–959.
53. Smirnov,S., Matray,T.J., Kool,E.T. and de los Santos,C. (2002) Integrity of duplex structures without hydrogen bonding: DNA with pyrene paired at abasic sites. *Nucleic Acids Res.*, **30**, 5561–5569.
54. Johar,Z., Zahn,A., Leumann,C.J. and Jaun,B. (2008) Solution structure of a DNA duplex containing a biphenyl pair. *Chem. Eur. J.*, **14**, 1080–1086.
55. Georgiadis,M.M., Singh,I., Kellett,W.F., Hoshika,S., Benner,S.A. and Richards,N.G.J. (2015) Structural basis for a six nucleotide genetic alphabet. *J. Am. Chem. Soc.*, **137**, 6947–6955.
56. Betz,K., Malyshev,D.A., Lavergne,T., Welte,W., Diederichs,K., Romesberg,F.E. and Marx,A. (2013) Structural insights into DNA replication without hydrogen bonds. *J. Am. Chem. Soc.*, **135**, 18637–18643.
57. Röthlisberger,P., Istrate,A., Marcaida Lopez,M.J., Visini,R., Stocker,A., Reymond,J.L. and Leumann,C.J. (2016) X-ray structure of a lectin-bound DNA duplex containing an unnatural phenanthrenyl pair. *Chem. Commun.*, **52**, 4749–4752.
58. Nielsen,C.B., Petersen,M., Pedersen,E.B., Hansen,P.E. and Christensen,U.B. (2004) NMR structure determination of a modified DNA oligonucleotide containing a new intercalating nucleic acid. *Bioconjug. Chem.*, **15**, 260–269.
59. Sukackaite,R., Grazulis,S., Bochtler,M. and Siksnys,V. (2008) The recognition domain of the BpujI restriction endonuclease in complex with cognate DNA at 1.3-angstrom resolution. *J. Mol. Biol.*, **378**, 1084–1093.
60. Sukackaite,R., Grazulis,S., Tamulaitis,G. and Siksnys,V. (2012) The recognition domain of the methyl-specific endonuclease McrBC flips out 5-methylcytosine. *Nucleic Acids Res.*, **40**, 7552–7562.
61. Bittermann,H., Siegemund,D., Malinovskii,V.L. and Häner,R. (2008) Dialkynylpyrenes: strongly fluorescent, environment-sensitive DNA building blocks. *J. Am. Chem. Soc.*, **130**, 15285–15287.

62. Winiger,C.B., Li,S., Kumar,G.R., Langenegger,S.M. and Häner,R. (2014) Long-distance electronic energy transfer in light-harvesting supramolecular polymers. *Angew. Chem. Int. Ed.*, **53**, 13609–13613.
63. Kabsch,W. (2010) Xds. *Acta Cryst.*, **D66**, 125–132.
64. Adams,P.D., Afonine,P.V., Bunkoczi,G., Chen,V.B., Davis,I.W., Echols,N., Headd,J.J., Hung,L.W., Kapral,G.J., Grosse-Kunstleve,R.W. *et al.* (2010) PHENIX: a comprehensive Python-based system for macromolecular structure solution. *Acta Cryst.*, **D66**, 213–221.
65. Emsley,P., Lohkamp,B., Scott,W. and Cowtan,K. (2010) Features and development of Coot. *Acta Cryst.*, **D66**, 486–501.
66. Qian,B., Raman,S., Das,R., Bradley,P., McCoy,A.J., Read,R.J. and Baker,D. (2007) High-resolution structure prediction and the crystallographic phase problem. *Nature*, **450**, 259–264.
67. Terwilliger,T.C., Grosse-Kunstleve,R.W., Afonine,P.V., Moriarty,N.W., Zwart,P.H., Hung,L.W., Read,R.J. and Adams,P.D. (2008) Iterative model building, structure refinement and density modification with the PHENIX AutoBuild wizard. *Acta Cryst.*, **D64**, 61–69.
68. Schüttelkopf,A.W. and van Aalten,D.M.F. (2004) PRODRG: a tool for high-throughput crystallography of protein-ligand complexes. *Acta Cryst.*, **D60**, 1355–1363.
69. Häner,R., Samain,F. and Malinovskii,V.L. (2009) DNA-assisted self-assembly of pyrene foldamers. *Chem. Eur. J.*, **15**, 5701–5708.
70. Leontis,N.B., Stombaugh,J. and Westhof,E. (2002) The non-Watson-Crick base pairs and their associated isostericity matrices. *Nucleic Acids Res.*, **30**, 3497–3531.
71. Nussbaumer,A.L., Samain,F., Malinovskii,V.L. and Häner,R. (2012) Supramolecular polymerization of oligopyrenotides—stereochemical control by single, natural nucleotides. *Org. Biomol. Chem.*, **10**, 4891–4898.
72. Neelakandan,P.P., Pan,Z., Hariharan,M., Zheng,Y., Weissman,H., Rybtchinski,B. and Lewis,F.D. (2010) Hydrophobic self-assembly of a perylenediimide-linked DNA dumbbell into supramolecular polymers. *J. Am. Chem. Soc.*, **132**, 15808–15813.
73. Sargsyan,G. and Balaz,M. (2012) Porphyrin-DNA conjugates: porphyrin induced adenine-guanine homoduplex stabilization and interduplex assemblies. *Org. Biomol. Chem.*, **10**, 5533–5540.
74. Spano,F.C. (2010) The spectral signatures of frenkel polarons in H- and J-aggregates. *Acc. Chem. Res.*, **43**, 429–439.